IEEE Access
Multidisciplinary | Rapid Review | Open Access Journal

Received July 28, 2019, accepted August 17, 2019, date of publication August 21, 2019, date of current version September 3, 2019.

Digital Object Identifier 10.1109/ACCESS.2019.2936617

High-Performance and High-Capacity Ultraviolet Communication With Orbital Angular Momentum

SUDHANSHU ARYA, (Student Member, IEEE), AND YEON HO CHUNG, (Senior Member, IEEE)
Department of Information and Communications Engineering, Pukyong National University, Busan 48513, South Korea

Corresponding author: Yeon Ho Chung (yhchung@pknu.ac.kr)

This work was supported by the Basic Science Research Program through the National Research Foundation of Korea (NRF) funded by the Ministry of Education under Grant 2018R1D1A3B07049858.

ABSTRACT In this paper, a high-performance and high-capacity ultraviolet (UV) communication system is presented using orbital angular momentum (OAM) of the Laguerre-Gaussian beam. It is well known that the Laguerre-Gaussian beams propagating along the same axis with different azimuthal states are mutually orthogonal. This orthogonality property allows OAM beams to be potentially useful in improving the performance of a UV communication system. In addition, an OAM beam with fixed angular momentum value could act as a data channel. We first derive a novel analytical expression for the UV channel impulse response considering the Laguerre-Gaussian beam with a fixed OAM mode value acting as a data channel. Based on this impulse response, novel expressions for average symbol error rate (ASER) and channel capacity are derived. It is shown via simulation that the proposed OAM based UV communication system achieves significantly higher error performance and higher channel capacity than conventional UV systems. It is also found that the received beam divergence is the main factor limiting the performance of the proposed system.

INDEX TERMS Average symbol error rate, Laguerre-Gaussian beam, ultraviolet.

I. INTRODUCTION

Wireless communication using electromagnetic (EM) waves carrying orbital angular momentum (OAM) has attracted increasing interest in recent years. An EM wave carrying OAM has a helical transverse phase structure of exp $(jl\phi)$, where ϕ is the transverse azimuthal angle and l is an unbounded OAM mode number. Beams carrying OAM with different l values are mutually orthogonal, allowing them to be multiplexed together along the same beam axis. This feature offers a new degree of freedom and the potential to increase the capacity [1], [2]. Unlike from the propagation mechanism of conventional radio frequency, the energy of OAM-carrying beam is focused within the bounded circle region surrounding the beam axis, which results in different propagation loss inside and outside the circle region [3].

Recently, the potential of OAM to increase the channel capacity has extensively been explored. As a method to improve the communication reliability, an OAM based multiuser access technique was presented with OAM states that act as new orthogonal dimensions for interference avoidance [4]. It was also demonstrated that the spectrum efficiency of a traditional frequency-division-multiple-access (FDMA) was lower than that achieved using the OAM based multiple access. The implementation of a Dammann optical vortex grating (DOVG) for the multiplexing of massive OAM states with individual modulation and demodulation was analyzed [5]. This work presented a significant gain in the channel capacity and also removed the bottleneck of massive OAM state parallel detection. In [6], an interesting OAM-based index modulation (OAM-IM) scheme was presented as a technique to improve the bit error performance with reduced system complexity. The OAM-IM used the activated OAM modes themselves to carry information through the principle of IM. This scheme was found to outperform the conventional OAM-based mode division multiplexing in terms of bit error performance. In [7], a similar interesting OAM-based spatial modulation (OAM-SM) scheme was also proposed for millimeter wave communication systems, where the OAM-SM based communication system outperforms the

The associate editor coordinating the review of this article and approving it for publication was Yuan Gao.

OAM-based multi-input multi-output system significantly in terms of the energy efficiency and is more suitable for long-range communication links.

Although the feasibility of OAM based free space communication was studied, there are many research problems unresolved. For example, because the electromagnetic wave with OAM is vorticose hollow and divergent [8], the OAM beam needs to be converged for relatively long distance transmission. Moreover, the phase error due to fading is hard to be estimated at the receiver. Although OAM beam is vorticose hollow and divergent, the divergence reduces greatly as the frequency increases. For this reason, it is expected to use OAM with high carrier frequency including visible light or ultraviolet band.

Ultraviolet (UV) communication has attracted much interest for applications in free space communication in recent years, because of its relative insensitivity to pointing errors and robustness against shadowing [9], [10]. In addition, UV performance and link range were further enhanced with various promising techniques [11]–[14]. Yet the strong absorption and scattering in the UV channel impose a temporal dispersion on the transmitted pulses. Thus, intersymbol interference and low received power can be factors limiting the performance in UV communication systems [15], [16]. To circumvent the above difficulty, we consider a UV communication system implemented with the Laguerre-Gaussian beam with a single fixed OAM state acting as a data channel. The main contributions of our work are listed as follows:

- A closed-form expression for the UV channel impulse response is derived, considering the radially polarized Laguerre-Gaussian beam with a fixed OAM state acting as a data channel.
- A closed-form analytical expression for the average symbol error rate (ASER) is derived.
- An analytical expression for the channel capacity is also presented.
- Impact of the OAM mode states and the radially polarized index on the performance is presented.

In this work, it should be noted that, irrespective of the OAM mode value of the Laguerre-Gaussian beam, the presence of a beam only represents the bit "1". That is, we consider the OAM-carrying Laguerre-Gaussian beam as a data channel to carry the bit "1". We do not employ the OAM multiplexing to transmit the data.

The remainder of the paper is organized as follows. Section II presents the signal model. Section III describes the configuration of transmitter and receiver structures. An analytical approach to evaluate ASER and the channel capacity is also presented. Results and discussions are provided in Section IV and conclusions are drawn in Section V.

II. SIGNAL MODEL

The Laguerre-Gaussian UV beam with constant OAM mode is considered to act as a data channel with bits "1" and "0" represented by the presence and absence of a beam, respectively. The system model is illustrated in Fig. (1).

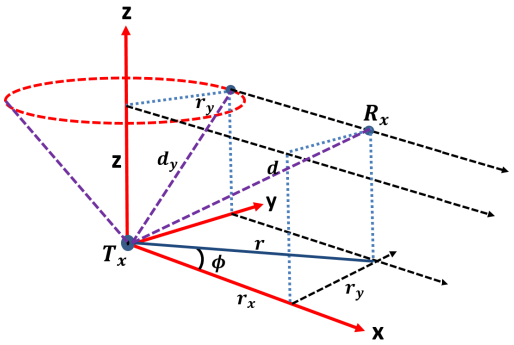

FIGURE 1. OAM based UV communication link in cylindrical coordinates.

The cylindrical coordinate system (r, ϕ, z) is utilized for the system analysis where we assume the reference plane is the Cartesian xy-plane with $z = 0$. r represents the radius of the cylindrical geometry formed, ϕ is the azimuth angle between the reference direction on the chosen plane and the line from the origin to the projection of the receiver R_x on the plane. z represents the axial distance from the transmitter to the receiver. The transmitting antenna T_x is assumed to be located at the coordinate $(0, 0, 0)$. d represents the distance between the transmitter and the receiver located at the coordinates (r, ϕ, z).

The electric field of the Laguerre-Gaussian beam is given by

$$\vec{E} = U(r, \phi, z)\hat{a}, \tag{1}$$

where $\hat{a}$ is a constant unit vector and the term $U(r, \phi, z)$ is given by [17]

$$\begin{aligned} &U(r, \phi, z) \\ &= \alpha \sqrt{\frac{p!}{\pi\,(p + |l|)!}} \frac{1}{w\,(z)} \left(\frac{\sqrt{2}r}{w\,(z)}\right)^{|l|} \\ &\quad \times L_p^{|l|}\left(\frac{2r^2}{w^2\,(z)}\right) \exp\left(-\frac{r^2}{w^2\,(z)}\right) \exp\left[-j\frac{z}{z_R}\left(\frac{r}{w\,(z)}\right)^2\right] \\ &\quad \times \exp\left[-j\,(|l| + 2p + 1)\,\varphi\,(z)\right] \exp\left(-jl\phi\right) \exp\left(-jkz\right) \end{aligned} \tag{2}$$

where p is the radial index, l is the topological charge (OAM state), and $w(z)$ is the Gaussian beam width defined as $w\,(z) = w_0\sqrt{1 + \left(\frac{z}{z_R}\right)^2}$, where w_0 is the minimum beam radius at $z = 0$. z_R is the Rayleigh range and is equal to $\frac{kw_0^2}{2}$, where k is the wavenumber. $(|l| + 2p + 1)\,\varphi\,(z)$ is the Gouy phase shift with $\varphi\,(z) = \tan^{-1}(z/z_R)$. $L_p^{|l|}$ is the generalized Laguerre polynomial of degree p and order l. It can be easily shown that for a constant value of a radial index p, the principle of orthogonality is satisfied [18]

$$\begin{aligned} &(U_l(r, \phi, z), U_m(r, \phi, z)) \\ &\quad \triangleq \int U_l(r, \phi, z) U_m^*(r, \phi, z) r dr d\phi \\ &\quad = \begin{cases} 0, & \forall m \neq l \\ \int |U_l(r, \phi, z)|^2\, r dr d\phi, & m = l, \end{cases} \end{aligned} \tag{3}$$

where the operator $(\cdot, \cdot)$ represents the scalar product and the operator $*$ denotes the complex conjugate.

The angular momentum density associated with the transverse electromagnetic field is expressed by [19]

$$\vec{M} = \varepsilon_0 \vec{r} \times \left(\vec{E} \times \vec{B}\right). \tag{4}$$

Using (4), the total angular momentum (consisting of the OAM and the spin angular momentum) of the Laguerre-Gaussian beam can then readily be obtained as

$$\vec{J} = \varepsilon_0 \int \vec{r} \times \left(\vec{E} \times \vec{B}\right) d\vec{r}. \tag{5}$$

The amplitude of Laguerre-Gaussian beam has an azimuthal angular dependence of $exp(-jl\phi)$ and carry an orbital angular momentum of lh [20].

A. CHANNEL IMPULSE RESPONSE

Assuming the distance d between the transmitter and the receiver, the channel impulse response can be modeled as [21]

$$h_p^l = \beta_p^l \frac{\lambda}{4\pi d} \exp\left(j\frac{2\pi d}{\lambda}\right) \exp\left(jl\phi\right), \tag{6}$$

where λ represents the wavelength of the UV signal and β_p^l is the channel gain coefficient which denotes the attenuation during the propagation of an OAM-carrying Laguerre-Gaussian UV beam. β_p^l can then be modeled as

$$\beta_p^l = \sqrt{G_s G_a \left|A_p^l(b,\theta)\right|^2}, \tag{7}$$

where the terms G_a and G_s denote the power attenuation due to the atmospheric absorption and scattering of the UV photons, respectively. $A_p^l(b,\theta)$ is the amplitude function of the Laguerre-Gaussian beam and is defined as [22]

$$A_p^l(b,\theta) = \left(\frac{k}{2\pi}\right)^2 \int_0^{\infty}\int_0^{2\pi} U(r,\phi,z) \exp\left[-jkbr\cos\left(\phi-\theta\right)\right] rd\phi dr \tag{8}$$

where b and θ are the angular spectrum variables [23].

On solving the double integration in Eq. (8), the closed form expression for $A_p^l(b,\theta)$ is derived as

$$\begin{aligned} A_p^l(b,\theta) &= \left(\frac{w_0}{\pi}\right) \times \exp\left[-j\left(|l|+2p+1\right)\varphi(z)\right] \\ &\quad \times \exp\left(-jl\frac{\pi}{2}\right) \exp\left(jl\theta\right) \\ &\quad \times \sum_{a=0}^{p} (-1)^a \left(\frac{2^{3/2}}{k}\right)^{|l|+2a} \frac{1}{b\left[bw(z)\right]^{|l|+2a+1}} \binom{p+l}{p-a} \\ &\quad \times \frac{1}{a!} G_{2,1}^{1,1}\left(\frac{4}{[w(z)kb]^2}\middle| \begin{matrix} -|l|-a, a \\ 0 \end{matrix}\right) \exp\left(-jkz\right) \end{aligned} \tag{9}$$

where $G_{e,f}^{g,h}(\cdot)$ represents the Miejer G function.

The attenuation due to the absorption G_a is modeled as exp(-$\alpha_a d$), whereas G_s can be expressed as exp($-\alpha_s d$), where

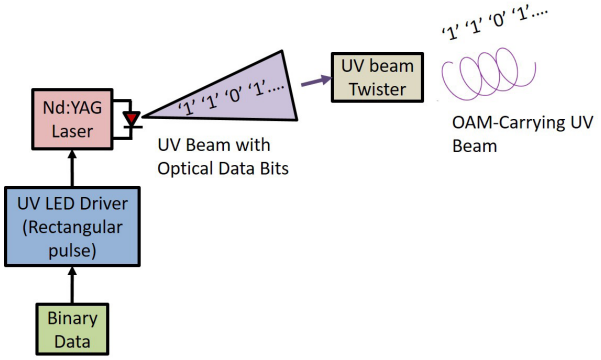

FIGURE 2. Structure of the transmitter.

α_a and α_s are atmospheric parameters called the absorption and scattering coefficients, respectively. These parameters determine the average distance that a UV photon travels before being absorbed or scattered [24]. Considering a homogeneous atmosphere, a UV photon experiences Rayleigh (due to air molecules) and Mie (due to aerosol particles) scatterings. These scattering are often jointly modeled in a single phase function of $\alpha_s = \alpha_{sr} + \alpha_{sm}$. α_{sr} is the Rayleigh scattering coefficient and is defined as [25]

$$\alpha_{sr} = \frac{24\pi^3[\mu^2-1]^2}{\lambda_{\mu m}^4 N[\mu^2+2]^2} \times \frac{6+3\rho_\mu}{6-7\rho_\mu}, \tag{10}$$

where $\lambda_{\mu m}$ denotes the wavelength of the OAM-carrying UV beam in micrometers. N is the molecular number density and ρ_μ is known as the depolarization ratio and is a function of the UV wavelength. μ is the refractive index of air, calculated at the UV wavelength $\lambda_{\mu m}$ and is given by the relation [25]

$$\mu - 1 = \left(8060.51 + \frac{2480990}{132.274-\lambda_{\mu m}^{-2}} + \frac{17455.7}{39.32957-\lambda_{\mu m}^{-2}}\right) \times 10^{-8}. \tag{11}$$

α_{sm} is defined as [26]

$$\alpha_{sm} = \left(\frac{3.912}{v} - \alpha_{sr(\lambda_{nm}=550)}\right) \times \left(\frac{\lambda_{nm}}{550}\right)^{0.585v^{1/3}}, \tag{12}$$

where λ_{nm} is the UV wavelength measured in nanometers and v is the atmospheric visibility in kilometers.

III. SYSTEM ANALYSIS

The transmitter is illustrated in Fig. (2). The binary data is first used to modulate the intensity of the UV carrier. Then, it employs a compact Q-switched fourth harmonic Nd:YAG laser which is triggered by a rectangular pulse from a signal generator, thereby producing a laser pulse train with the pulse width of (3-5) nano-seconds. To generate a helical phase front, a spiral phase plate (SPP) antenna is employed, which provides small divergence and low attenuation of the OAM signal. Because of a helical phase front of an OAM-carrying UV beam, it results in a twisting wave-vector as shown in Fig. (2). Owing to the helical phase pattern, the beam

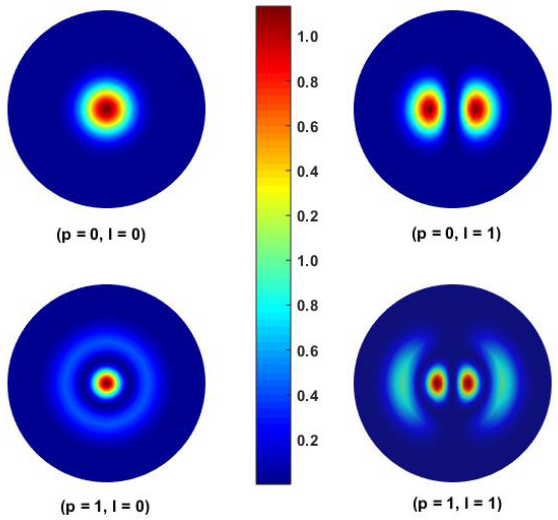

FIGURE 3. Normalized intensity distribution of various LG modes at UV wavelength.

typically has an annular ring intensity profile with a phase singularity at the beam center, as depicted in Fig. (3). Every OAM mode has a ring-shaped intensity profile depending upon the radial index p value with $p + 1$ rings. The intensity profile is represented by using Laguerre-Gaussian distribution. For example, with $p = 1$, the OAM mode has two rings and the phase difference between the rings is π. This phase difference of π will result in destructive interference in the focal region at the receiver.

At the receiver, as shown in Fig. (4), we assume that an objective lens with a refractive index of 1 is used for the focusing of an incident beam. Based on the vector diffraction study, it is predicted that a smaller spot is achievable by the tight focusing of a radially polarized Laguerre-Gaussian beam [27]. On increasing the radial index p, the number of rings increases in the focal plane. Generally, the outermost ring of the Laguerre-Gaussian beam is relatively wide, suggesting that a significant amount of the beam energy is distributed to this outermost ring [28]. Therefore, the contribution of the outermost ring to the beam focusing must be important. For the correct reading of the photodiode, a transimpedance amplifier circuit is employed.

When a radially polarized optical light is focused by an objective lens, the electric field component in the tangential (azimuthal) direction becomes zero and the total composite electric field in the focal region consists of two components i.e., the transverse (radial) component E_r and the longitudinal (axial) component E_z. These components near the focus region can readily be obtained as

$$E_r(r,\phi,z) = C\int_0^{\tau_{\max}} A_p^l(b,\theta)\sqrt{\cos(\tau)}\sin(2\tau)J_1[kr\sin(\tau)] \times \exp[ikz\cos(\tau)]\,d\tau, \quad (13)$$

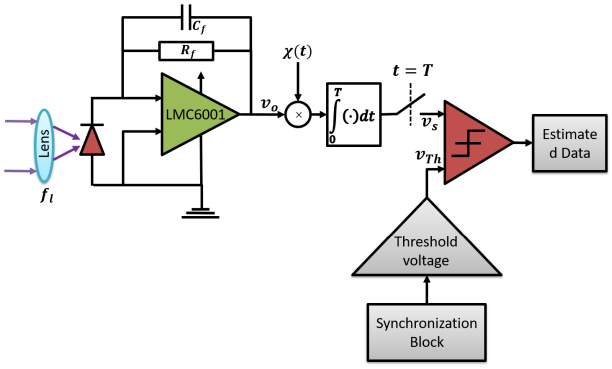

FIGURE 4. Structure of the receiver.

and

$$E_z(r,\phi,z) = i2C\int_0^{\tau_{\max}} A_p^l(b,\theta)\sqrt{\cos(\tau)}\sin^2(\tau)J_0[kr\sin(\tau)] \times \exp[ikz\cos(\tau)]\,d\tau. \quad (14)$$

$\tau_{\max}$ in (13) and (14) represents the maximum angle of the numerical aperture of the objective lens. C is the constant, and J_0 and J_1 represent the Bessel functions of first kind with order 0 and 1, respectively.

The output sequence is related to the input sequence by

$$y(n) = \sum_{q=-\infty}^{\infty} h_p^l(n-q)\,x(q) + w_n(n), \quad (15)$$

where $x(n)$ is the input bit stream. $w_n(n)$ is the sequence of independent and identically distributed Gaussian random variables, with $\mathbf{E}[w_n(n)] = 0$.

A. OPTIMUM THRESHOLD VALUE AND ASER

As shown in Fig. (4), the unit energy basis function $\chi(t)$ is modeled as

$$\chi(t) = \begin{cases} \frac{1}{\sqrt{T}}, & 0 \le t \le T \\ 0, & \text{otherwise} \end{cases}. \quad (16)$$

Using (16), the conditional probability density function (PDF) of the sampled outputs is obtained as

$$f(v_s|x=0) = \frac{1}{\sqrt{2\pi\sigma_n^2}}\exp\left(-\frac{v_s^2}{2\sigma_n^2}\right) \quad (17)$$

and

$$f(v_s|x=1) = \frac{1}{\sqrt{2\pi\sigma_n^2}}\exp\left\{-\frac{\left(v_s - \frac{\sqrt{P_t T}\beta_p^l\lambda}{\sqrt{8}\pi d}\right)^2}{2\sigma_n^2}\right\}. \quad (18)$$

where P_t is the transmitted optical power. Assuming that the transmitted signals are equally probable, the decision rule

may be expressed as

$$\frac{\exp\left(-\frac{v_s^2}{2\sigma_n^2}\right)}{\exp\left\{-\frac{\left(v_s-\frac{\sqrt{P_tT}\beta_p^l\lambda}{\sqrt{8}\pi d}\right)^2}{2\sigma_n^2}\right\}} \begin{matrix} x_0 \\ > \\ < \\ x_1 \end{matrix} 1. \tag{19}$$

Using Eq. (19), the optimum threshold value is then given by

$$v_{Th} = \frac{\sqrt{P_tT}\beta_p^l\lambda}{\sqrt{32}\pi d}. \tag{20}$$

The ASER for equally probable transmission can be written as

$$ASER = \frac{1}{2}\int_{v_{Th}}^{\infty} f(v_s|x=0)\,dv_s + \frac{1}{2}\int_{-\infty}^{v_{Th}} f(v_s|x=1)\,dv_s. \tag{21}$$

On substituting Eqs. (17), (18), and (20) into (21) and also solving for the integration, the ASER is derived as

$$ASER = Q\left(\sqrt{\frac{P_tT}{\sigma_n^2}}\frac{\beta_p^l\lambda}{\sqrt{32}\pi d}\right). \tag{22}$$

B. CHANNEL CAPACITY ANALYSIS

As a basis for the capacity gain, the proposed system needs a certain transmit power to achieve a minimum threshold level of the received signal for different propagation distances. Using (6), the minimum required transmit power can be calculated as

$$P_{t,\min} = P_r\left(\frac{4\pi d}{\beta_p^l\lambda}\right)^2. \tag{23}$$

In general, it is important to note that the time scales of the fading are far larger than the transmitted bit interval. h_p^l can therefore be considered constant over a larger amount of transmitted bits. In addition, the delay spread in a UV channel can be neglected as it is on the order of one hundred nanoseconds [29]. Therefore, assuming the narrowband flat-channel with $h_p^l(n) = h_p^l$, we obtain the discrete transfer function of the channel impulse response as

$$H_p^l(\Omega) = \sum_{n=0}^{\infty} h_p^l(n)\,e^{-j\Omega n}, \quad -\pi \le \Omega \le \pi$$
$$H_p^l(\Omega) = \frac{h_p^l}{1-e^{-j\Omega}} + \sum_{k=-,\infty}^{\infty} \pi\delta(\Omega - 2\pi k), \quad -\pi \le \Omega \le \pi \tag{24}$$

Using Eq. (24), the capacity of the OAM-carrying UV beam can be derived as [30]

$$C = \frac{1}{4\pi}\int_{-\pi}^{\pi} \max\left[0, \log_2\left(\frac{K_p}{\Gamma(\Omega)}\right)\right]d\Omega \tag{25}$$

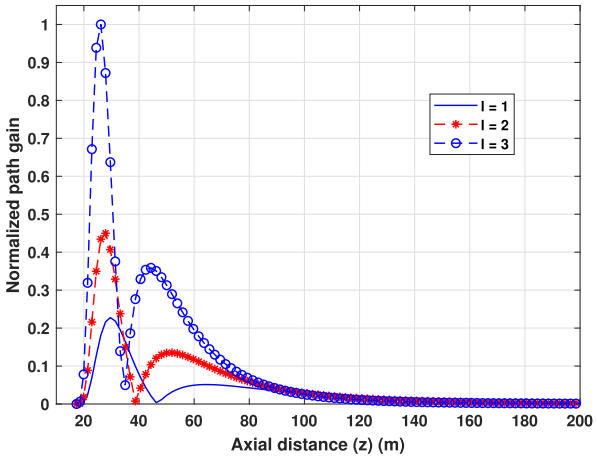

FIGURE 5. Normalized path gain relative to axial distance ($p = 1$).

where K_p can be deduced from the expression

$$P_t = \frac{1}{2\pi}\int_{-\pi}^{\pi} \max\left[0, K_p - \Gamma(\Omega)\right]d\Omega \tag{26}$$

and $\Gamma(\Omega)$ is given by the expression

$$\Gamma(\Omega) = \left[H_p^l(\Omega)\right]^{-1}\sigma_n^2\left\{\left[H_p^l(\Omega)\right]^{-1}\right\}^*, \quad -\pi \le \Omega \le \Omega \tag{27}$$

where the operator $*$ represents the conjugate operation.

IV. SIMULATION RESULTS AND ANALYSIS

A UV wavelength equal to 260 nm is considered for the communication link. α_{sr} and α_{sm} are obtained using (10), (11), and (12). α_a is set to 0.802 km^{-1} [24]. v is set to 21 km. Both r_x and r_y are set to 5 m. The molecular number density N is equal to 2.4481 $\times$ 10^{25} m^{-3}, given the air pressure of 1013 hPa and temperature of 300 K [25]. At λ equal to 260 nm, the depolarization ratio ρ_μ is 3.501 $\times$ 10^{-2} [25].

An important metric is how molecular scattering and absorption affect the OAM-carrying Laguerre-Gaussian UV beam. Fig. (5) illustrates the normalized path gain of the channel as a function of axial distance. The path gain is normalized to the peak value. It is interesting to note that the minimum value corresponds to the UV optical cage consisting of a dark region surrounded by an intense UV field near the focal point. In addition, as expected, the amplitude of the OAM based UV channel impulse response decreases as the transmission distance increases. This substantial decrease indicates that the amplitude of the OAM-carrying Laguerre-Gaussian UV beam is highly attenuated by molecular scattering and absorption, thereby potentially impairing the detection performance at the receiver as the distance increases. It should also be noted that as the OAM state value l increases, the normalized path gain increases. This is due to the fact that a larger l value results in a larger beam size at the receiver, therefore resulting in a higher path gain.

The performance dependence of the proposed system on the topological charge l and the radial index p is illustrated

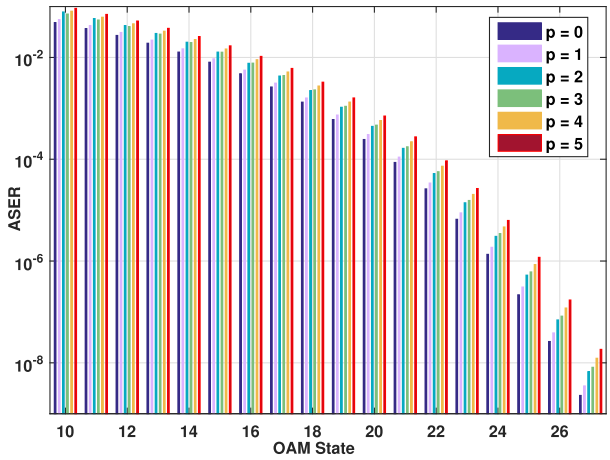

FIGURE 6. ASER relative to the OAM state for different radial indexes p.

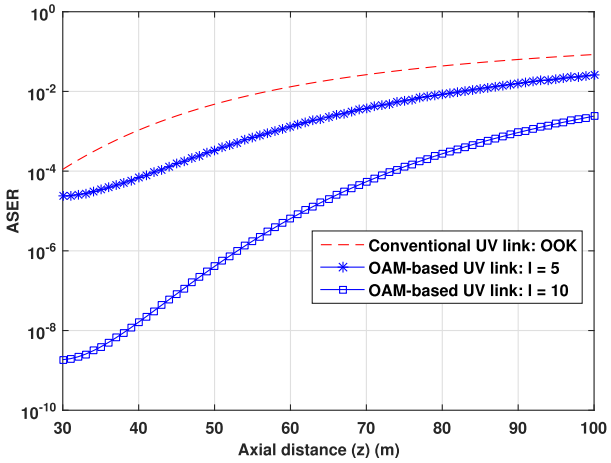

FIGURE 7. ASER relative to axial distance ($p = 1$).

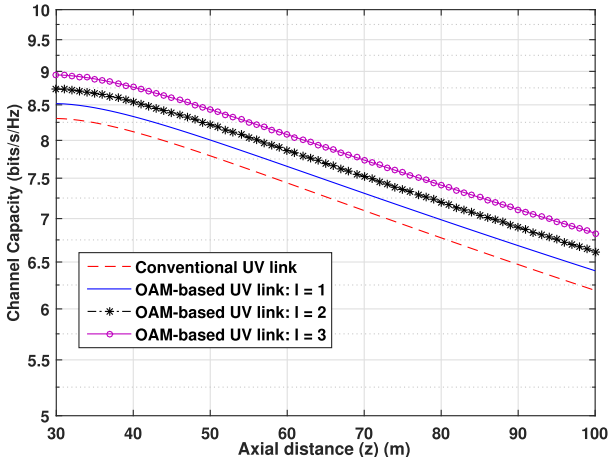

FIGURE 8. Achievable channel capacity relative to axial distance for different OAM states.

in Fig. (6). At a fixed radial index p value, the OAM beams have ring shaped intensity profiles for different l values with zero or low intensity at the center and radii of the outer ring proportional to $\sqrt{(l)}$. Since the outermost ring of an OAM-carrying Laguerre-Gaussian UV beam is relatively wide, a significant amount of the total beam energy is distributed to the outermost ring. For example, for a particular case of $p = 1$ and $l = 5$, the intensity at the center is nearly zero with the outermost ring containing 44.4 percent of the total beam energy [28]. Because the significant amount of total beam energy is distributed to the outermost ring, the outermost ring is important for the performance of the system. We employed an objective lens to focus the energy of the outermost ring on the receiver. The tightly focused outermost ring of Laguerre-Guassian beam results in a spot formation at the receiver. As a result, as OAM state increases with p fixed, the size of the outermost ring increases with lower destructive interference, thereby resulting in higher received energy at the receiver. This higher received energy with increased l leads to a higher received SNR and a lower ASER.

In addition, from Fig. (6), it can also be seen that the ASER increases with the radial index p. This can be attributed to the fact that as p increases, the spot size decreases in the focal region because of the destructive interference caused by the longitudinal electric field components of the inner rings to the outermost ring. For example, in particular, a radially polarized UV beam with $p = 2$ can effectively reduce the focal spot size because of 180° phase shift between the inner and the outer ring. Note that the radial index p indicates a degree of radial polarization. That is, a larger value of p means a higher level of divergence (lower received intensity). Since the number of rings for Laguerre-Gaussian beam increases with p, the influence of the inner rings increases, leading to a decrease in the focal spot size due to an increase in the destructive interference, thereby resulting in lower received optical power and higher ASER.

Fig. (7) compares the proposed OAM-carrying UV beam with a conventional UV communication employing on-off keying (OOK) modulation in terms of the ASER performance. As can be seen, the ASER performance degrades with the transmission distance. The substantial decrease in the performance with increasing distance is attributed to the fact that as the distance increases, the amplitude of the channel impulse response decreases, thereby attenuating the transmitted OAM-carrying UV beam. However, it is important to note that the performance of the OAM-carrying UV beam is still superior to the conventional UV communication system without OAM. The propagation pattern of OAM beams is different from that of the conventional UV beam link, as the energy of the OAM beam is focused within a circular region surrounding the beam axis. This results in different propagation gains inside and outside the circle region. This characteristic is found to contribute the outperformance of the OAM-based UV link over the conventional UV link.

In Fig. (8), the achievable capacity of the OAM-based UV communication system is depicted against the axial distance, considering different OAM states. When the transmission distance is fixed, the capacity of the OAM-based UV system increases with the increasing OAM mode. That is, a larger OAM state l value results in a larger beam size at the receiver

and therefore the received power increases, thus providing a higher capacity. It is also apparent that for increased distances, less power will be received at the receiver aperture due to the divergence of the OAM beam and higher path loss.

V. CONCLUSION

In this paper, a free space wireless channel model for the Laguerre-Gaussian UV beam with the fixed OAM mode has been considered. The exact closed-form expressions for the ASER and the channel capacity have first been derived. Based on these novel expressions, the performance and capacity have been analyzed. It is demonstrated that the OAM-carrying UV communication system outperforms the conventional UV communication system in terms of the performance and capacity. The received beam divergence is found to be a limiting factor as the distance increases. This limitation is, however, envisioned to be readily addressed by employing multiple receivers.

REFERENCES

[1] A. E. Willner, H. Huang, Y. Yan, Y. Ren, N. Ahmed, G. Xie, C. Bao, L. Li, Y. Cao, and Z. Zhao, "Optical communications using orbital angular momentum beams," *Adv. Opt. Photon.*, vol. 7, no. 1, pp. 66–106, Mar. 2015.
[2] Y. Yan, G. Xie, M. P. Lavery, H. Huang, N. Ahmed, C. Bao, Y. Ren, Y. Cao, L. Li, and Z. Zhao, "High-capacity millimetre-wave communications with orbital angular momentum multiplexing," *Nature Commun.*, vol. 5, Mar. 2014, Art. no. 4876.
[3] L. Wang, X. Ge, R. Zi, and C.-X. Wang, "Capacity analysis of orbital angular momentum wireless channels," *IEEE Access*, vol. 5, pp. 23069–23077, 2017.
[4] W. Cheng, W. Zhang, H, Jing, S. Gao, and H. Zhang, "Orbital angular momentum for wireless communications," *IEEE Wireless Commun.*, vol. 26, no. 1, pp. 100–107, Feb. 2019.
[5] T. Lei, M. Zhang, Y. Li, P. Jia, G. N. Liu, X. Xu, Z. Li, C. Min, J. Lin, and C. Yu, "Massive individual orbital angular momentum channels for multiplexing enabled by Dammann gratings," *Light, Sci. Appl.*, vol. 4, no. 3, 2015, Art. no. e257.
[6] E. Basar, "Orbital angular momentum with index modulation," *Trans. Wireless Commun.*, vol. 17, no. 3, pp. 2029–2037, Mar. 2018.
[7] X. Ge, R. Zi, X. Xiong, Q. Li, and L. Wang, "Millimeter wave communications with OAM-SM scheme for future mobile networks," *IEEE J. Sel. Areas Commun.*, vol. 35, no. 9, pp. 2163–2177, Sep. 2017.
[8] B. Thidé, H. Then, J. Sjöholm, K. Palmer, J. Bergman, T. D. Carozzi, Y. N. Istomin, N. H. Ibragimov, and R. Khamitova, "Utilization of photon orbital angular momentum in the low-frequency radio domain," *Phys. Rev. Lett.*, vol. 99, no. 8, 2007, Art. no. 087701.
[9] Z. Xu and B. M. Sadler, "Ultraviolet communications: Potential and state-of-the-art," *IEEE Commun. Mag.*, vol. 46, no. 5, pp. 67–73, May 2008.
[10] T. Y. Aung, S. Arya, and Y. H. Chung, "Performance dependence of non-line-of-sight ultraviolet communications on atmospheric parameters of the ultraviolet channel," *Opt. Commun.*, vol. 443, pp. 7–11, Jul. 2019.
[11] S. Arya and Y. H. Chung, "Spectrum sensing for free space optical communications in strong atmospheric turbulence channel," *Opt. Commun.*, vol. 445, pp. 24–28, Aug. 2019.
[12] S. Arya and Y. H. Chung, "Generic blind spectrum sensing scheme for all optical-wavelength multi-user free space optical communications," *Opt. Commun.*, vol. 450, pp. 316–321, Nov. 2019.
[13] S. Arya and Y. H. Chung, "A novel blind spectrum sensing technique for multi-user ultraviolet communications in atmospheric turbulence channel," *IEEE Access*, vol. 7, pp. 58314–58323, 2019.
[14] S. Arya and Y. H. Chung, "Amplify-and-forward multihop non-line-of-sight ultraviolet communication in the gamma–gamma fading channel," *J. Opt. Commun. Netw.*, vol. 11, no. 8, pp. 422–436, 2019.
[15] H. Ding, G. Chen, A. K. Majumdar, B. M. Sadler, and Z. Xu, "Modeling of non-line-of-sight ultraviolet scattering channels for communication," *IEEE J. Sel. Areas Commun.*, vol. 27, no. 9, pp. 1535–1544, Dec. 2009.
[16] S. Arya and Y. H. Chung, "Non-line-of-sight ultraviolet communication with receiver diversity in atmospheric turbulence," *IEEE Photon. Technol. Lett.*, vol. 30, no. 10, pp. 895–898, May 15, 2018.
[17] I. B. Djordjevic, J. A. Anguita, and B. Vasic, "Error-correction coded orbital-angular-momentum modulation for FSO channels affected by turbulence," *J. Lightw. Technol.*, vol. 30, no. 17, pp. 2846–2852, Sep. 1, 2012.
[18] J. A. Anguita, M. A. Neifeld, and B. V. Vasic, "Turbulence-induced channel crosstalk in an orbital angular momentum-multiplexed free-space optical link," *Appl. Opt.*, vol. 47, no. 13, pp. 2414–2429, May 2008.
[19] J. D. Jackson, *Classical Electrodynamics*. 3rd ed. New York, NY, USA: Wiley, 1999.
[20] D. Marcuse, *Light Transmission Optics*. New York, NY, USA: Van Nostrand, 1972.
[21] Z. Zhang, S. Zheng, Y. Chen, X. Jin, H. Chi, and X. Zhang, "The capacity gain of orbital angular momentum based multiple-input-multiple-output system," *Sci. Rep.*, vol. 6, May 2016, Art. no. 25418.
[22] C. J. Bouwkamp, "Diffraction theory," *Rep. Prog. Phys.*, vol. 17, no. 1, p. 35, 1954.
[23] A. Cerjan and C. Cerjan, "Orbital angular momentum of Laguerre–Gaussian beams beyond the paraxial approximation," *J. Opt. Soc. Amer. A, Opt. Image Sci.*, vol. 28, no. 11, pp. 2253–2260, 2011.
[24] D. M. Junge, "Non-line-of-sight electro-optic laser communications in the middle ultraviolet," Ph.D. dissertation, Naval Postgraduate School, Monterey, CA, USA, 1977.
[25] C. Tomasi, V. Vitale, B. Petkov, A. Lupi, and A. Cacciari, "Improved algorithm for calculations of Rayleigh-scattering optical depth in standard atmospheres," *Appl. Opt.*, vol. 44, no. 16, pp. 3320–3341, 2005.
[26] E. M. Patterson and J. B. Gillespie, "Simplified ultraviolet and visible wavelength atmospheric propagation model," *Appl. Opt.*, vol. 28, no. 3, pp. 425–429, 1989.
[27] S. Quabis, R. Dorn, M. Eberler, O. Glöckl, and G. Leuchs, "Focusing light to a tighter spot," *Opt. Commun.*, vol. 179, nos. 1–6, pp. 1–7, 2000.
[28] Y. Kozawa and S. Sato, "Focusing of higher-order radially polarized Laguerre–Gaussian beam," *J. Opt. Soc. Amer. A, Opt. Image Sci.*, vol. 29, no. 11, pp. 2439–2443, 2012.
[29] Q. He, B. M. Sadler, and Z. Xu, "Modulation and coding tradeoffs for non-line-of-sight ultraviolet communications," *Proc. SPIE*, vol. 7464, 2009, Art. no. 74640H.
[30] L. H. Brandenburg and A. D. Wyner, "Capacity of the Gaussian channel with memory: The multivariate case," *Bell Syst. Tech. J.*, vol. 53, no. 5, pp. 745–778, May/Jun. 1974.

SUDHANSHU ARYA (S'19) received the M.Tech. degree in communications and networks from the National Institute of Technology, Rourkela, India, in 2017. He is currently pursuing the Ph.D. degree in optical communication with Pukyong National University, Busan, South Korea. His research interests include free-space optical communication, cognitive radio networks, and physical-layer security.

YEON HO CHUNG (M'93–SM'17) received the M.Sc. degree from Imperial College London, U.K., in 1992, and the Ph.D. degree from the University of Liverpool, U.K., in 1996. He was a Visiting Professor with Pennsylvania State University, University Park, USA, and also with Chiba University, Japan. He was a Foreign Expert for the GIAN Program of the Government of India, in 2017. He is currently a Professor with the Department of Information and Communications Engineering, Pukyong National University, Busan, South Korea. His research interests include visible light communications, optical wireless communications, optical healthcare systems, and advanced mobile transmission schemes. He is a member of the Editorial Board of the International Journal of *Wireless Personal Communications* (Springer) and *Internet Technology Letters* (Wiley). He received the Top 2014 Paper Award from the *Transactions on Emerging Telecommunications Technologies* (ETT) (Wiley) and the Best Paper Award from the ICUFN 2019, Croatia. He is an Associate Editor of IEEE Access.